

# Electronic supplementary information for: A microfluidic platform for quantitative measurements of effective protein charges and single ion binding in solution

Therese W. Herling, Paolo Arosio, Thomas Müller, Sara Linse, and Tuomas P. J. Knowles

Received Xth XXXXXXXXXXXX 20XX, Accepted Xth XXXXXXXXXXXX 20XX

First published on the web Xth XXXXXXXXXXXX 200X

DOI: 10.1039/b000000x

## 1 Microfluidic device preparation

Microfluidic devices were fabricated using standard soft lithography methods.<sup>1</sup> The devices were cast in polydimethylsiloxane, PDMS, (Sylgard 184, Dow Corning, OneCall, UK) which was coloured black by the addition of 0.2% w/w carbon nanopowder prior to curing (Sigma, UK). The electrodes were integrated by placing the bonded device glass slide down on a hot plate set to 79° C and inserting InBiSn alloy (51% In, 32.5% Bi, 16.5% Sn, Conro Electronics, UK) through the solder inlet, Fig. 2(a).<sup>2</sup> As shown in Fig. 2(a) the microfluidic devices contained two sets of pillar arrays: one for the electrode alignment and the other to support the ceiling of the wide central channel. When these electrodes were operated under flow, electrolysis products were carried away at a rate exceeding their formation, thus preventing their accumulation beyond their solubility limit and the formation of gas bubbles within the microfluidic channels. This key feature of the experimental protocol enabled the continuous operation of an electric field.<sup>2</sup>

## 2 Expression and purification of calbindin

Calbindin D<sub>9k</sub> site directed mutagenesis was performed and the protein constructs were purified recombinantly as previously recorded.<sup>3–5</sup> To prevent cis-trans isomerisation constructs c8, c9, c10, and c14 contained the P43M substitution.<sup>6</sup> The constructs were labelled with Alexa488. The protein samples were incubated for three hours in 20 mM sodium phosphate buffer, pH 8.0, at room temperature under gentle agitation with maximum one equivalent of Alexa488 carboxylic acid succinimidyl ester to covalently label primary amines. Following the labelling reaction excess dye was removed by desalting on a G25 gel filtration column, followed by purification by anion exchange to remove any protein with multiple labels, and an additional desalting step on a G25 gel filtration column before use. The purity of the samples was verified by

NMR spectroscopy, SDS PAGE, and agarose gel electrophoresis, Fig. 4(c).

## 3 Free-flow electrophoresis measurements

Fluorescence images for both the diffusion and electrophoresis experiments were recorded using a CCD camera (Evolve 512, Photometrics, Arizona, US) through inverted optics (Observer D1, Zeiss, UK). Diffusion and electrophoresis measurements for each sample were performed under two sets of buffer conditions, 5 mM Tris-HCl pH 8.0 with either 0.1 mM CaCl<sub>2</sub> or 0.1 mM EDTA acid. Unless otherwise stated chemicals for buffer solutions were purchased from Sigma UK.

The image acquisition and current measurements by a digital multimeter (34401A, Agilent Technologies, California, US) were triggered through the auxiliary output of a lock-in amplifier (SR830, Stanford Research Systems, California, US), which was also used to apply an electric potential. The flow rate through the device was set to 500  $\mu\text{L hr}^{-1}$  (neMESYS syringe pump, Cetoni, Germany) and controlled by withdrawal through the outlet using a glass syringe (Hamilton Switzerland), Fig. 2(a). In our calculation of  $v_d$  we considered the lower flow velocities at the channel boundaries.<sup>7</sup> These result in a higher average flow velocity in the central region of the channel, where the lateral migration of sample molecules occurs. The high aspect ratio of the channels allows an even sample distribution in the vertical direction. We evaluated the average flow rate in the central region of the channel to be 519.6  $\mu\text{L hr}^{-1}$  and used this value to calculate the sample residence time between the electrodes to be 3.4 s.

Four repeats of a voltage ramp of 0 to 4 V at 0.5 V intervals were applied for each sample, with three image acquisitions and current readings per step. The resulting position of the sample fluorescence intensity maximum and current were measured, Fig. 2(d).

Calibration of the cell constants and buffer conductivities

were performed using a lock-in amplifier as reported previously.<sup>2</sup> In brief, a conductivity standard,  $500 \mu\text{S cm}^{-1}$  (Sigma, UK) or a buffer solution was flowed through the device to be calibrated at a flow rate of  $500 \mu\text{L hr}^{-1}$ , a 10 mV AC voltage was applied with a variable frequency from 10 Hz to 100 kHz. Measurements were made of the resulting current, and thus the admittance, as a voltage drop over a  $220 \Omega$  resistor. At frequencies above 1 kHz, the conductance of the solution within the channel limited the overall current flow resulting in a plateau in the admittance. The conductances of the solutions were then determined from the constant part of the spectrum.

From the measured conductance of the conductivity standard, we were able to determine the cell constant, allowing us to determine the buffer conductivity and thereby the electric field corresponding to each current measurement, Fig. 2(f). Electrophoresis data analysis was performed using software written in python. The electrophoretic mobilities of the solvated proteins were determined by a linear fit to the deflection velocity against electric field, Fig. 2(f) and (g).

## 4 Diffusion measurements

The electrophoretic mobility of each construct is determined by the effective net charge of the migrating molecule,  $q$ , and diffusion coefficient,  $D$ , of the solvated protein,

$$\mu_e = \frac{qD}{k_B T}, \quad (1)$$

where  $k_B$  and  $T$  are the Boltzmann constant and absolute temperature respectively. We used this simple and well-defined relationship to determine the net charge of the calbindin constructs in solution.

Previous studies indicate that the binding of  $\text{Ca}^{2+}$  does not lead to considerable structural changes in of the protein calbindin  $\text{D}_{9k}$ .<sup>8</sup> To investigate whether the variations in amino acid sequence and solution conditions affected the size of the constructs we performed microfluidic diffusion experiments to measure the diffusion coefficient of each construct in both the EDTA and  $\text{Ca}^{2+}$  buffers, Fig. 3.

The low Reynolds number of liquids in micron scale channels results in the laminar flow of solutions within microfluidic channels. Therefore the only lateral movement of solvated species occurs via diffusion and thus depends on the particle size and the diffusion time. For a spherical particle with radius,  $R_a$ , the diffusion coefficient is described by the Stokes-Einstein equation

$$D = \frac{k_B T}{6\pi\eta R_H}, \quad (2)$$

where  $\eta$  is the viscosity of the solution. This observation has enabled the use of measurements of analyte diffusion

within microfluidic channels to determine the diffusion coefficient of and separate particles in solution, Fig. 3(a).<sup>9–12</sup>

In order to determine the size of the calbindin constructs we used simulated sample profiles for particles with diffusion coefficients corresponding to radii of 0.1–10 nm. The propagation of particles with a range of diffusion coefficients were simulated under laminar Poiseuille flow through the channel dimensions shown in Fig. 3(a) with no-slip boundary conditions.<sup>12</sup> The diffusion coefficient and profile, dashed lines in Fig. 3(b), best describing the observed sample diffusion, green lines in Fig. 3(b), was found through least squares fitting using 100 steps of the basin-hopping algorithm<sup>13</sup> with 2500 iterations at each step. Fits to the data were performed using software written in python. We observed convergence and a good fit to the data for every sample.

For each construct diffusion profiles were acquired at three different flow rates:  $80 \mu\text{L/hr}^{-1}$ ,  $120 \mu\text{L/hr}^{-1}$ , and  $160 \mu\text{L/hr}^{-1}$ . The simulations were performed for a flow rate of  $160 \mu\text{L/hr}^{-1}$ . The flow rates were controlled by withdrawal through the device outlet, Fig. 3(a). During the data analysis the residence times were therefore corrected accordingly for the experiments performed at lower flow rates. We arrived at very similar diffusion coefficients for each flow rate, the error bars in Fig. 3(c) represent the standard deviation between the three flow rates.

## 5 Zeta potential

The electrophoretic mobility can be related to the the zeta potential,  $\zeta$ , of the migrating ion. In this study we investigate a relatively small protein at low ionic strength,  $I$ , thus the Debye length,  $\lambda_d$ , is comparable to the protein size. Under this condition of a thick double layer, the Hückel equation relates the electrophoretic mobility to the zeta potential,

$$\mu_p = \frac{2\epsilon_0\epsilon_R\zeta}{3\eta}, \quad (3)$$

where  $\epsilon_R$  is the relative permittivity of the medium and  $\epsilon_0$  the permittivity of free space, SI Fig 1.<sup>14</sup>

The findings presented here are in good agreement with the non-linear relationship proposed by Loeb, Overbeek, and Wiersema between the dimensionless zeta-potential,  $\tilde{\zeta}$ ,<sup>14</sup>

$$\tilde{\zeta} = \frac{e\zeta}{k_B T}, \quad (4)$$

and the surface charge,  $Q_e$ ,

$$Q_e = 4\pi\epsilon_0\epsilon_R \frac{k_B T}{ze} \frac{a^2}{\lambda_d} \left( 2\sinh(z\tilde{\zeta}/2) + \frac{4\lambda_d}{a} \tanh(z\tilde{\zeta}/4) \right) \quad (5)$$

We note that  $Q_e$  is the charge at the shear plane and thus distinct from the effective charge of the migrating species,  $q$ ,

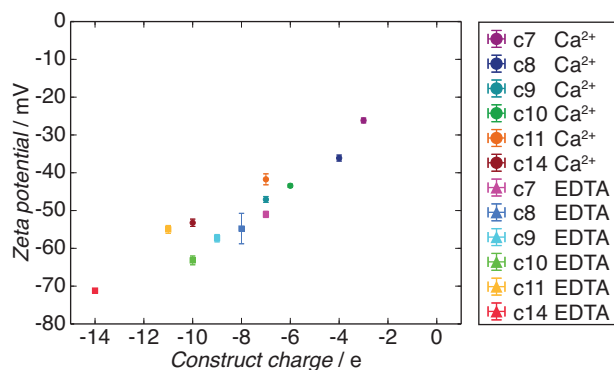


**Fig. 1** SI Figure 1. Zeta potential. The zeta potentials of the calbindin constructs determined from the measured electrophoretic mobilities using equation 3. Were these colloids the calculated values would indicate that the stability of the constructs are intermediate to good. However, as the proteins, unlike most colloidal systems, carry both positive and negative charges the stability cannot necessarily be assessed directly based on the zeta potential.

and the naked protein charge in the absence of all counter ions. This relation predicts a plateau in the zeta potential as the surface charge increases. Where  $a$  is the distance to the shear plane,  $a = R_a + \lambda_d$ , and  $z$  the valency of the counter ions. The Debye length is found from the following relation to the ionic strength,  $I$ ,

$$\lambda_d = \sqrt{\frac{\epsilon_R \epsilon_0 k_B T}{N_A e^2 I}}. \quad (6)$$

Here  $N_A$  and  $e$  represent the Avogadro number and elementary charge respectively, and  $e$  is the elementary charge.

Unlike colloidal particles carrying a uniformly distributed charge, proteins such as calbindin carry both positively and negatively charged groups, which are not necessarily evenly distributed on the protein surface. We have therefore not used the colloidal model directly to describe proteins in solution, but to provide qualitative insights into the expected trends only.

## References

- 1 J. C. McDonald and G. M. Whitesides, *Acc. Chem. Res.*, 2002, **35**, 491–499.
- 2 T. W. Herling, T. Müller, L. Rajah, J. N. Skepper, M. Vendruscolo and T. P. J. Knowles, *Appl. Phys. Lett.*, 2013, **102**, 184102.
- 3 S. Linse, P. Brodin, T. Drakenberg, E. Thulin, P. Sellers, K. Elmdén, T. Grundström and S. Forsén, *Biochemistry*, 1987, **26**, 6723–6735.
- 4 S. Linse, C. Johansson, P. Brodin, T. Grundström, T. Drakenberg and S. Forsén, *Biochemistry*, 1991, **30**, 154–162.
- 5 P. Brodin, C. Johansson, S. Forsén, T. Drakenberg and T. Grundström, *J. Biol. Chem.*, 1990, **265**, 11125–11130.
- 6 A. L. Svensson, E. Thulin and S. Forsén, *Jour. Mol. Biol.*, 1992, 601–606.
- 7 M. G. L. Spiga M, *Int. Commun. Heat Mass*, 1994, **21**, 469–475.
- 8 N. J. Skelton, J. Kordel, M. Akke, S. Forsén and W. J. Chazin, *Nat. Struct. Mol. Biol.*, 1994, **1**, 239–245.
- 9 A. E. Kamholz, B. H. Weigl, B. A. Finlayson and P. Yager, *Anal. Chem.*, 1999, **71**, 5340–5347.
- 10 A. Hatch, A. E. Kamholz, K. R. Hawkins, M. S. Munson, E. A. Schilling, B. H. Weigl and P. Yager, *Nat. Biotech.*, 2001, **19**, 461–465.
- 11 A. E. Kamholz, E. a. Schilling and P. Yager, *Biophys. J.*, 2001, **80**, 1967–1972.
- 12 C. T. Culbertson, S. C. Jacobson and J. Michael Ramsey, *Talanta*, 2002, **56**, 365–373.
- 13 D. J. Wales and J. P. K. Doye, *J. Phys. Chem. A*, 1997, **101**, 5111–5116.
- 14 R. J. Hunter, *Zeta Potential in Colloid Science: Principles and Applications*, Academic Press, New York and London, 1981.